Available online at www.sciencedirect.com
ScienceDirect
Journal of Computational Physics 227 (2008) 6372–6384
JOURNAL OF COMPUTATIONAL PHYSICS
www.elsevier.com/locate/jcp

On the consistency of the direct forcing method in the fractional step solution of the Navier–Stokes equations

Federico Domenichini *

Dipartimento Ingegneria Civile e Ambientale, Università di Firenze, Via S. Marta 3, 50139 Firenze, Italy

Received 26 April 2007; received in revised form 22 February 2008; accepted 11 March 2008
Available online 20 March 2008

Abstract

In the present work the application of the direct forcing method to the fractional step solution of the Navier–Stokes equations is analyzed in details. The central topic of the study is the satisfaction of the boundary conditions in the presence of immersed bodies. To this aim, simple two-dimensional problems with steady forcing and sharp-edged surfaces are solved with a standard fractional step method. It is shown that the direct forcing scheme is not able to satisfy the impenetrability condition. This fact appears to be strictly related to the use of fractional step methods. A mathematically based explanation is given, suggesting that improvements can be obtained with the iterative solution of the irrotational part of the flow, when spectral methods are used and local modification of the discrete differential operators are difficult to be implemented. The results are then verified in two-dimensional unsteady problems and three-dimensional flows with moving smooth boundaries.

Keywords: Navier–Stokes equations; Immersed boundaries methods; Direct forcing method

1. Introduction

In the last years, computational fluid dynamics has received a renewed impulse from the continuous advancement of the numerical techniques. Among the other developments, it is worthy to be reminded the refinement of the immersed-boundary methods (IB), which allow the simulation of flows with immersed bodies on regular grids that are not conformal to the shape of the boundaries. The IB methods include a large variety of numerical techniques (see Mittal and Iaccarino [1] and references therein for a review) that can be used in conjunction with finite-differences, finite-volume and finite-element approaches.

In any case, the central point of the IB methods is the imposition of the boundary conditions at the surface of immersed bodies. These conditions can be included into the system of continuous equations or, alternatively, into the discrete one, giving the continuous and discrete forcing approaches, respectively [1]. The former was introduced for the simulation of viscous flows and elastic immersed boundaries [2], and it is based on the

* Tel.: +39 0554796471; fax: +39 055495333.
E-mail address: federico.domenichini@unifi.it

0021-9991/$ - see front matter © 2008 Elsevier Inc. All rights reserved.
doi:10.1016/j.jcp.2008.03.009

Eulerian–Lagrangian description of the fluid and solid variables, respectively. The interpolation of the fluid quantities gives the motion and the deformation of the bodies, from these the Lagrangian distribution of stresses acting on them can be computed. On the opposite, these stresses are spread and transformed in the Eulerian force density, which is considered in the solution of the Navier–Stokes equation. The kernel function for the Eulerian–Lagrangian transformation, the Dirac δ function, is replaced numerically by different smoother ones (see [2,3] for examples). This method, which appears well suited for flow with elastic boundaries, has been subsequently modified and adapted for the presence of rigid bodies.

The discrete forcing approach can be further divided into two classes, characterized by the indirect or the direct imposition of the boundary conditions. The first method is based on the determination of the forcing terms from the fluid solution [4–6]. With the direct forcing method, the boundary conditions are imposed directly at the IB, usually requiring the local modification of the computational stencil. Different approaches have been developed to be used with finite-difference and finite-volume techniques ([1], and references therein).

In the present work we discuss the application of the direct forcing method to the numerical solution of the Navier–Stokes equation with mixed spectral-finite-differences methods. Several works have been devoted to develop the direct forcing method in the finite-differences framework, they was mainly focused on the accuracy of the solution close to the boundaries. Different schemes for the local interpolation of the fluid velocities have been tested, linear (bi- and tri-linear) and/or quadratic interpolations are typically used [1].

One of the most interesting aspect is represented by the application of the direct forcing when a fractional step method is used to solve the governing equations; this is a well-known two-steps method where the momentum equation is advanced in time giving an intermediate non-solenoidal field, then the mass conservation is enforced solving a Poisson problem for the pressure or for an irrotational corrective field [7,8]. The attractiveness of the direct forcing method stands in its easy implementation: during the temporal advancement, the kinematical conditions are imposed at (near) the boundaries with different interpolating schemes, avoiding the solution of additional equations for the forcing term. The intriguing point is represented by the straightforward solution of the Poisson equation, without the imposition of specific conditions at the boundaries [9].

Independently on the particular scheme adopted for the time advancement of the Navier–Stokes equation, the velocity values at the boundaries are commonly enforced on the intermediate non-solenoidal field, instead of on the divergence-free one that is obtained at each time step after the imposition of the mass conservation. If this second step changes the velocity values at the immersed boundaries, the boundary conditions would be violated. Since the irrotational step consists in the solution of a Poisson problem and additional conditions are not imposed at the boundaries, there is no warranty about the correctness of the solution. This fact is independent on the spatial discretization used and on the specific method employed to impose the kinematical conditions. Such a crucial point was discussed by Fadlun et al. [9], which speculated that the correctness, in an approximate sense, of the solution could be related to the linearization of the velocities close to the boundary, that gives a negligible normal component of the pressure gradient, and, therefore, a negligible normal component of the irrotational correction.

More recently, a mass source term was introduced in the pressure equation to satisfy the mass balance in the computational cells cut by the walls [10], but such a method does not guarantee the satisfaction of the adherence condition. Alternatively, a method based on the local modification of the discrete operators (gradient and divergence) has been proposed, giving a consistent scheme for the irrotational part of the solution [11]. In this work, it is not clear whether the same interpolation operator is used for both momentum and pressure (irrotational part of the solution) equations or not, because the latter one can not satisfy the adherence, but only the impenetrability condition.

The present work is focussed on the study of the boundary conditions when the direct forcing method is used in the numerical solution of the equations that rule incompressible viscous flows. More precisely, the central issue is the satisfaction of the impenetrability condition in correspondence of fixed and moving walls. In order to drive the discussion far from specific numerical details (interpolating procedures, local accuracy, *et cetera*) towards the basic problem of the consistency of the approach, simple two-dimensional problems with rigid boundaries are studied. Afterwards, the analysis is extended to the three-dimensional flow inside an expanding cavity.

2. Mathematical formulation and numerical method

Some problems involving the incompressible motion of a viscous fluid are considered. The governing equations in dimensionless form read

$$\frac{\partial \boldsymbol{v}}{\partial t} + \boldsymbol{v}\nabla\boldsymbol{v} = -\nabla p + Re^{-1}\nabla^2\boldsymbol{v}, \tag{1}$$

$$\nabla \cdot \boldsymbol{v} = 0, \tag{2}$$

where $\boldsymbol{v}$ and p are the velocity vector and the pressure field, respectively. The Reynolds number $Re = UL/v$ is defined depending on the specific problem under consideration; v is the kinematic viscosity of the fluid, L and U are a length and a velocity scale, respectively. Three-dimensional problems are assumed to be periodic in the x and y directions of a Cartesian system of coordinates. Along these, Fourier expansions are used to describe the flow variables. Two-dimensional flows are periodic in the x direction.

The system (1-2) is solved numerically with a fractional step method. A spectral representation of the variables is used along the periodic directions; second-order centered finite-differences are employed for the spatial discretization along z. In case of two-dimensional problems, the results reported below have been obtained with an analogous version of the numerical code entirely based on finite differences, giving undistinguishable results. Eq. (1) is advanced in time using a third-order low-storage Runge–Kutta scheme, giving the intermediate non-solenoidal field $\boldsymbol{v}^*$; apart from the coefficients that must be used to advance the single sub-time step, omitted for brevity, the procedure can be synthesized as

$$\frac{\boldsymbol{v}^* - \boldsymbol{v}^n}{\Delta t} = -\mathcal{G}(p^n) - \mathcal{H}(\boldsymbol{v}^n) + Re^{-1}\mathcal{N}(\boldsymbol{v}^n), \tag{3}$$

where the superscript indicates the instant of integration, Δt is the time step, $\mathcal{G}$ and $\mathcal{N}$ are the discrete gradient and Laplacian operators, respectively, $\mathcal{H}$ represents the non-linear term. The mass conservation (2) is imposed solving the Poisson-type problem (4) for the field ϕ, which is used to update the pressure and to correct the velocity field with the irrotational contribute $\mathcal{G}(\phi)$ [8]:

$$\mathcal{D}(\boldsymbol{v}^*) = \mathcal{D}\mathcal{G}(\phi^{n+1}), \tag{4}$$

$$p^{n+1} = p^n + \phi^{n+1}/\Delta t + O(\Delta t^2), \tag{5}$$

$$\boldsymbol{v}^{n+1} = \boldsymbol{v}^* - \mathcal{G}(\phi^{n+1}), \tag{6}$$

where $\mathcal{D}$ is the discrete divergence operator. The two-dimensional results reported below have been obtained with the explicit treatment of $\mathcal{N}(\boldsymbol{v}^n)$ in (3); same cases have been recalculated with an implicit method, showing identical results. The time step Δt has been always selected in order to satisfy the viscous and convective stability conditions.

3. Results

3.1. Test #1

Consider the two-dimensional problem in Fig. 1a. The flow is forced by a uniform velocity profile $v_z(x, 1) = -1$. The Reynolds number is $Re = U_0 L/v$, L is the dimensional width of the domain, U_0 the dimensional reference velocity. The solid fixed body is a square of side $d = 1/2$, placed symmetrically inside the domain.

The inlet profile is imposed to the intermediate field $\boldsymbol{v}^*$. The body surface corresponds to coordinate lines, where the normal component of the velocity (impenetrability) is imposed directly without any interpolation, e.g. point A in Fig. 1b for v_z^*. The tangential velocity at the points closest to the wall comes from the linear interpolation in the normal direction: $v_z^*(Z_1) = v_z^*(Z_2)/3$, Fig. 1c. A zero value of the velocity is imposed at the grid points inside the body. When (4) is solved, a homogeneous Neumann's condition is used at $z = 1$, so that the vertical component of $\mathcal{G}(\phi)$ does not modify the inlet profile. The Dirichlet's condition $\phi = 0$ is imposed at $z = 0$. The same conditions hold for the pressure p. Following the direct forcing approach [9],

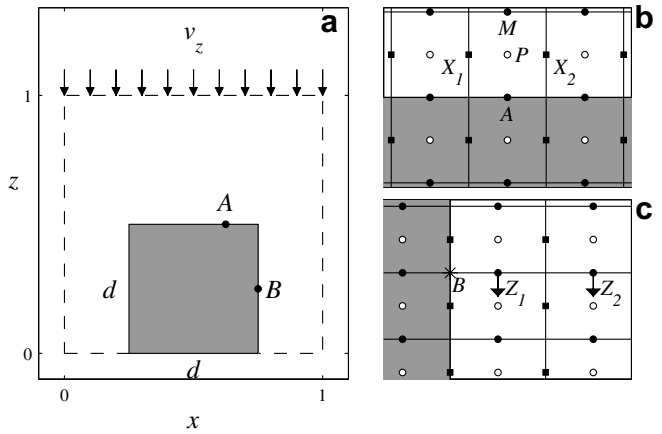

Fig. 1. (a) Sketch of the two-dimensional problem. (b and c) Computational grid close to the walls. Grid points for v_z (●), for v_x (■), for the pressure (○).

any condition is imposed at the body surface neither when $\mathcal{G}(p)$ is computed in (3) nor when the Poisson problem (4) is solved. The reference run was performed with $Re = 500$, time step $\Delta t = 1/512$, and a grid $N_x = N_z = 128$; then, the parameters have been varied as reported in Table 1. Two different initial conditions have been used: in the runs from #1 to #8 the flow starts from the rest, in the other cases the irrotational solution, satisfying the correct boundary conditions at the wall, has been used. This has been obtained with a modified version of the numerical code. A zero value is assigned to the component of $\mathcal{G}(\phi)$ normal to the walls when the velocity field is updated (6), the same condition is imposed explicitly in the Poisson solver (4), similarly to the method proposed in [11]. This code has been also used to perform a complete simulation; let us assume this solution, run #0, as"exact".

The comparison between the vorticity obtained with the direct forcing method and that of the exact solution, run #0, is reported in Fig. 2; the numerical parameters are those of run #1 in Table 1. The small differences between the vorticity distributions are due to the incorrect behavior of the solution at the upper side of the body, where the direct forcing method allows a flux through the wall. This leads to a reduction of the lateral flows, of the order of 5% in this case, which is sufficient to slightly modify the boundary-layer profile, and therefore the vorticity distribution. Grid refinements do not modify substantially the picture, only giving a smoother description of the flow field.

Table 1
Test #1: parameters of the runs. Initial condition: runs from #1 to #8, the flow starts from the rest; runs from #9 to #13, irrotational solution

#	Re	Δt	N_x	N_z
1	500	1/512	128	128
2	1000	1/512	128	128
3	250	1/512	128	128
4	500	1/1024	128	128
5	500	1/2048	128	128
6	500	1/512	256	128
7	500	1/1024	256	128
8	500	1/512	128	256
9	500	1/512	128	48
10	500	1/512	128	64
11	500	1/512	128	128
12	500	1/512	128	256
13	500	1/1024	128	512

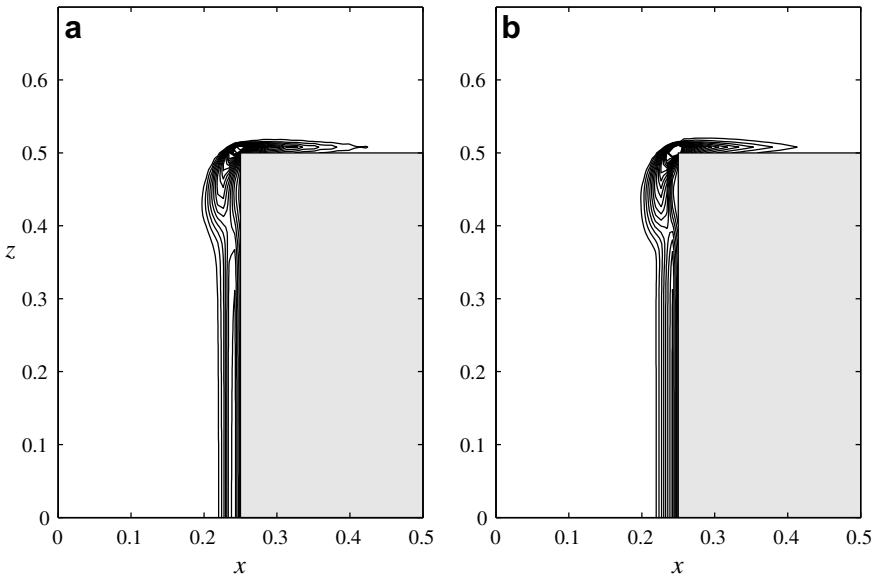

Fig. 2. Vorticity fields at $t = 4/64$. Run #1 in Table 1, direct forcing method (a); same numerical parameters, impenetrability condition imposed directly (b). Contour levels from -200 to -10, step 10.

In order to analyze the solution at and close to the walls, let us first discuss the behavior of the tangential velocity, point B in Fig. 1c. The temporal evolution of the linear extrapolation of the velocities at the points Z_1 and Z_2 in Fig. 1c, that would match the desired boundary condition $v_z(B) = 0$, is reported in Fig. 3. The initial evolution, $t < 0.2$, shows that the velocity rapidly decreases from its unitary value to ones that are four orders of magnitude smaller. Afterwards, the velocity changes sign and for $t > 1$ approaches an asymptotic value. Variations of the Reynolds number do not affect sensibly the solution until the thickness of the boundary-layer becomes relevant and influences a larger part of the flow domain, Fig. 3a. Smaller time steps give an initial more rapid decreasing of the velocity toward the zero value and lower asymptotic values, while a finer grid

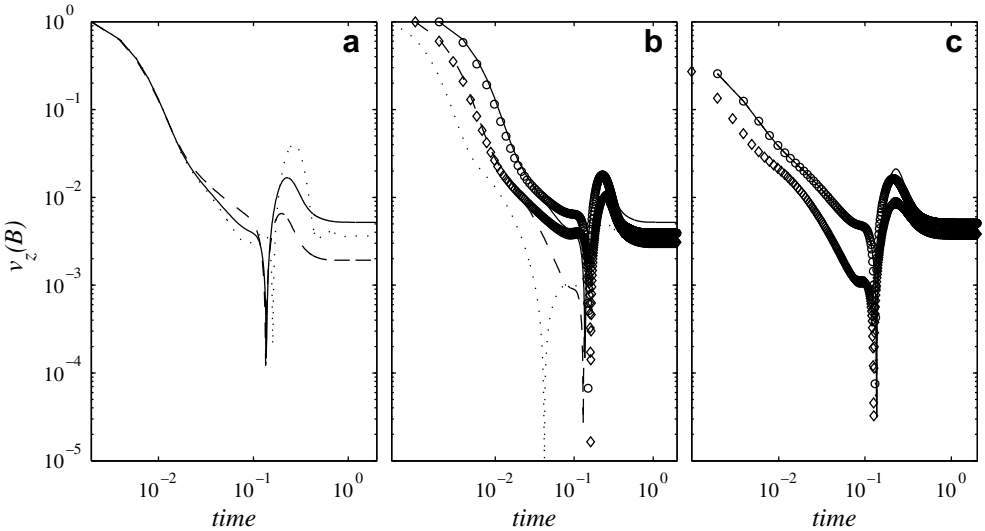

Fig. 3. Modulus of the tangential velocity at point B. (a) Continuous, dotted, dashed lines: runs #1, #2, #3 in Table 1, respectively. (b) Continuous line run #1, dashed line run #4, dotted line run #5, (○) run #6, (◇) run #7. (c) Continuous line run #9, dashed line run #10, dotted line run #11, (○) run #12, (◇) run #13.

along the x-direction has a negligible influence, Fig. 3b. Moreover, in Fig. 3c it is shown that a different initial condition and grid refinements along the z-direction do not modify substantially the solution.

An analogous behavior has been observed for the normal component of the velocity at the wall, which is analyzed in Fig. 4 referring to the point A in Fig. 1b. The solutions rapidly converge to asymptotic values that differ from the boundary (zero) condition imposed during the step (3). The convergence is rapid but not instantaneous, and it is almost independent on the viscous diffusion that takes place in the boundary-layer, see Fig. 4a where the results obtained with different Reynolds numbers are compared with that found solving with the same numerical code the inviscid version of the problem. In this case, given the steadiness of the forcing, the correct irrotational solution could be instantaneous, as that used as initial condition for the runs from #9 to #13. Then, the steps of the numerical integration necessary to reach the final state can be regarded as subsequent iterations. The solution is weakly influenced by grid refinements, compare runs #1, #6, and #8 in Fig. 4b and those in Fig. 4c, obtained with a different initial condition. A more evident dependence on the time step can be observed in Fig. 4b: the value of the solution and the interval of time for the rapid convergence are related almost inversely to Δt.

Results in Figs. 3 and 4 show that the direct forcing approach coupled with the fractional step method does not guarantee the satisfaction of the boundary conditions and that the error of the tangential velocity is approximately one order of magnitude smaller than that of the normal velocity. From a theoretical point of view, the field ϕ, steps (4) and (6), must be forced to ensure the impenetrability of the walls. On the opposite, any condition is imposed using the direct forcing method, where (4) is solved straightforwardly and the normal component of $\nabla\phi$ in (6) is computed accordingly. It must be noted that step (4) does not differ from its standard numerical implementation, where any condition is imposed in the tangential direction, following correctly the mathematical nature of the problem. At point B, the Navier–Stokes equation (1) reads $\partial p/\partial z = Re^{-1}\partial^2 v_z/\partial x^2$, the balance between the tangential pressure gradient and the normal variation of the shear stress. This holds exactly at the wall and approximately inside the boundary layer, where the convective term is typically small but not zero. In general, the viscous term is different from zero, thus $\partial p/\partial z \neq 0$. A zero tangential pressure gradient is in fact related to very particular cases, e.g. the Stokes's flows generated by the motion of a flat plate [12]. It can not be expected in more complex problems, such as flows over curved surfaces, as erroneously reported in [9]. Note that the condition $\partial p/\partial z \neq 0$ holds for inviscid flows also, where pressure gradient is necessary to support the tangential convection. Given the relationship (5) between ϕ and p, $\partial\phi/\partial z \neq 0$ is a natural condition for the irrotational correction. From a numerical point of view, as

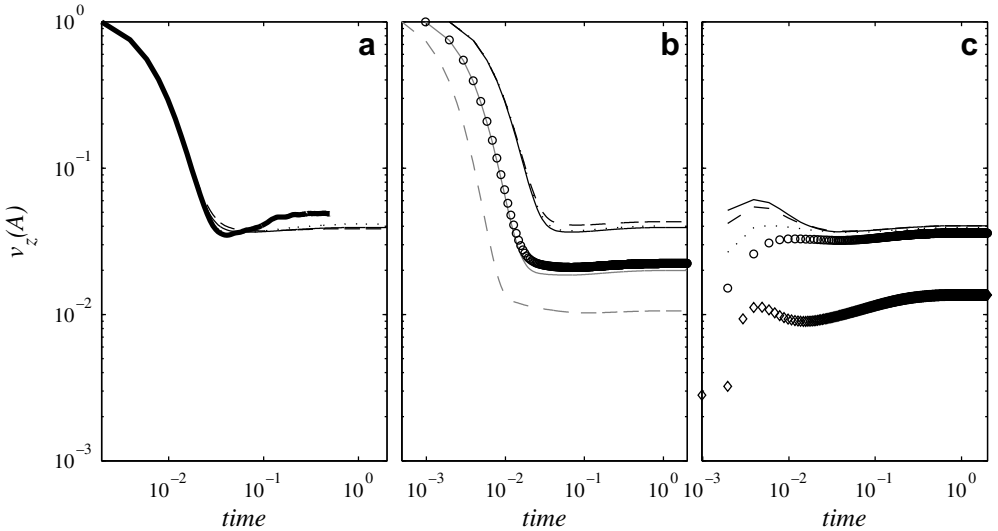

Fig. 4. Modulus of the normal velocity at point A. (a) Continuous, dotted, dashed lines: runs #1, #2, #3 in Table 1, respectively; thick line Euler (inviscid) solution. (b) Continuous line run #1, dashed line run #6, dotted line run #8, continuous gray line run #4, dashed gray line run #5, (○) run #7. (c) Continuous line run #9, dashed line run #10, dotted line run #11, (○) run #12, (◇) run #13.

it is standard when staggered grids are used, this contribute is computed at points inside the fluid domain, therefore the no-slip condition is not violated. Thus it can be argued that the error in the solution may be due to the inconsistency between the numerical approach and the physical constraint in the normal component of the velocity. In fact, results in Figs. 3 and 4 show that the error is almost independent on the grid resolution, while the numerical scheme has a global second-order accuracy in the space. It this therefore evident that the error at the wall comes from a conceptual inconsistency. On the opposite, it must be remarked the dependence of the solution on the time step of integration. Initially, the solution is almost irrotational, that is the sum of the fields ϕ, or $\mathcal{G}(\phi)$, computed at each time step. Having in mind the inviscid case reported in Fig. 4a it appears that the numerical integration needs some iterations to converge to the final value. Using a smaller Δt, the same iterations (the same number of irrotational fields) correspond to an interval of time proportionally smaller, as can be depicted in Fig. 4b, compare runs #1, #4, #5. Since different time steps slightly modify the evolution, the solutions show some little differences. Halving Δt, the convergence is accelerated by a factor that is a little greater than two.

This outcome becomes clearer if the algorithm is modified as follows: at the end of each time step, the boundary conditions are imposed, and steps (4)–(6) are repeated iteratively. The results of this numerical experiment are reported in Fig. 5 for different numbers of iterations. Additional irrotational fields give a more rapid convergence of the solution to the correct zero value, as suggested in [9]. Consider the computational cell close to the point A in Fig. 1b. The flow starts from the rest, then after the first step of the temporal advancement (3) $v_z(A) = 0$ (suppose for the sake of simplicity to force the mass conservation only at the end of the step (3) and not during the sub-steps of integration); only the points close to the inlet section are influenced by the advancement (3) because of the imposition of the inlet condition, while in the remaining part of the flow domain the velocity is zero. Thus, the divergence field is zero everywhere, with the exception of the computational cells at the inlet. Since any condition is imposed at the walls solving the Poisson problem, the solution after (4)–(6), satisfying the mass conservation, is the solenoidal uniform vertical flow $v_x = 0$ and $v_z = -1$, which does not satisfy the impenetrability condition, being $v_z(A) = -\partial\phi/\partial z|_A = -1$. If the boundary condition is imposed again, that is setting $v_z(A) = 0$, the first (standard) irrotational contribution is eliminated giving a field that satisfies the boundary condition, but adding a divergence at point $P, \mathcal{D}(P) = -\partial\phi/\partial z|_A/\Delta z = -1/\Delta z$. In other words, the flux through the surface at A, satisfying the mass conservation but violating the boundary condition, is replaced by a source in P. This procedure does not modify neither the velocity nor the divergence at the fluid points far from the boundaries. At the solid points, the velocity is modified being forced to be zero,

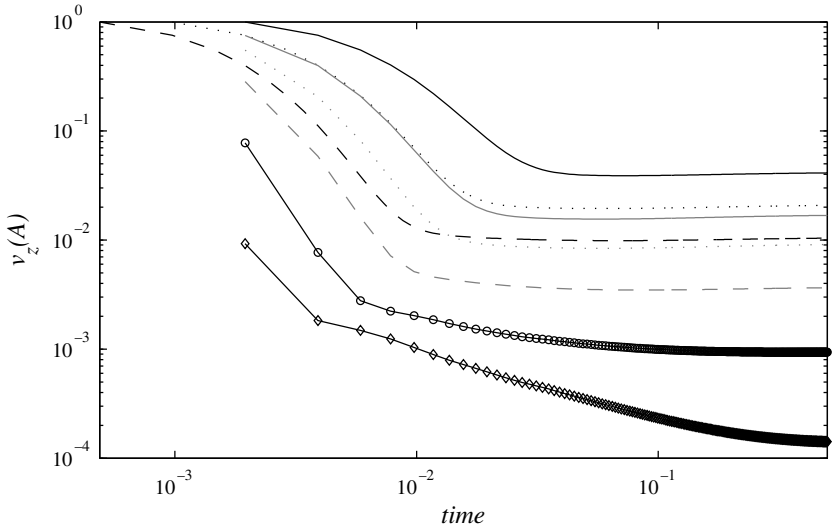

Fig. 5. Modulus of the normal velocity at point A. Continuous black, dotted black, dashed black lines runs #1, #4, #5 in Table 1, respectively. Continuous gray, dotted gray, dashed gray, (○), (◇) lines, same parameters of run #1 with 1, 2, 4, 8, 16 iterations of the irrotational correction, respectively.

while the divergence in the corresponding cells maintains the null value. Solving again (4) the divergence $\mathcal{D}(P)$, as well as that in the other cells close to the body, is newly eliminated. The new (second) irrotational field removes $\mathcal{D}(P)$ with different fluxes across the four sides of the cell. These are vertical (normal to the wall) at points A and M, and tangential at X_1 and X_2. The first flux through the boundary given by the first solution of (4) is therefore divided in four smaller fluxes. The velocity at point A is lowered of some percentages at each iteration, reducing the violation of the boundary condition.

To fix ideas, call $c_0 = v_z(A) = -1$ the velocity at the end of the numerical integration (3)–(6), the subscript now represents the iteration. After the first iteration, the normal velocity at A can be written $c_1 = \alpha c_0, \alpha < 1$ is the percentage of c_0 (of $\mathcal{D}(P)$) adsorbed by the lower side of the cell. If α was a constant, after the nth iteration we could write $c_n = \alpha^n c_0$, that is the knowledge of α would give an estimate of the celerity of the convergence. The distribution of c in correspondence of the upper border of the body are reported in Fig. 6a for some iterations computed after the first step of the integration (3)–(6), the numerical parameters are those of run #1. The velocity modulus decreases more rapidly in the middle of the border, with a slower convergence at the edges where higher values of α are found, Fig. 6b. This depends on the local stronger forcing due to the presence of the lateral walls, where the impenetrability is violated in the x-direction also. Smaller corrections are found at points inside the fluid domain ($x < 0.25$ and $x > 0.75$), where the divergence is not forced during the iterations. Notwithstanding the variability of α, a rough estimate of the rate of convergence of the process can be obtained with a single iteration.

3.2. Test #2

The same problem of Test #1 has been solved with a different treatment of the body. The points inside the body have been left free to develop a flow: the solid is a rigid square having sides of zero-thickness. Several runs have been made, see Table 2, with a Reynolds number $Re = 500$.

The evolution of the velocity at point A is reported in Fig. 7a. The previous findings are confirmed: smaller time steps improve the solution, and additional corrections help in reducing the violation of the boundary condition. It appears that when thin walls are considered, strictly speaking of zero thickness, the satisfaction of the boundary condition becomes a more crucial issue. The straightforward solution of (4) does not prove to be sufficiently accurate, compare the top line in Fig. 7a with the thick one, obtained in Test #1 with the same numerical parameters. With this treatment of the body, the impenetrability of the walls is violated more than before, being the normal velocity one order of magnitude higher than that found in Test #1. The flux across

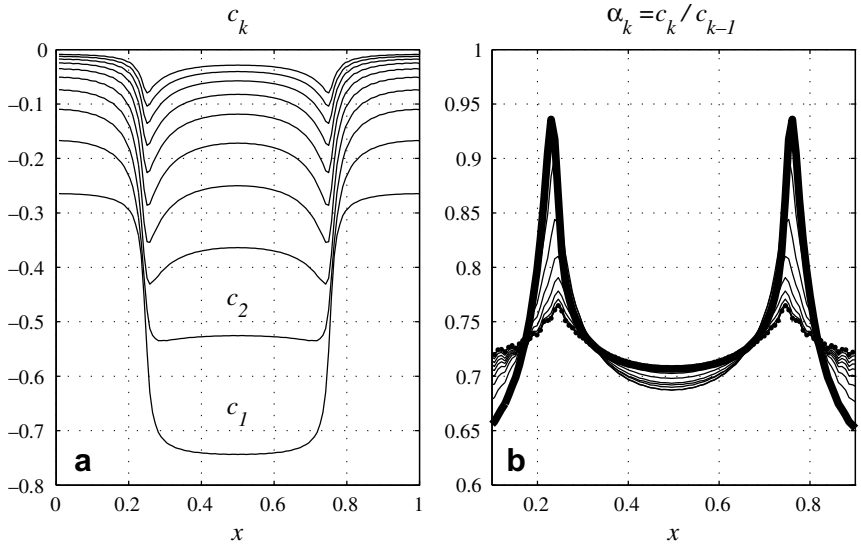

Fig. 6. (a) Vertical velocity c_k given by the iterations, at $z = 1/2$. (b) Ratio $\alpha_k = c_k/c_{k-1}$ between subsequent corrections. The thick line is α_1.

Table 2
Test #2: parameters of the runs

#	Δt	N_x	N_z	N
1	1/512	128	128	0
2	1/1024	128	128	0
3	1/2048	128	128	0
4	1/512	128	128	1
5	1/512	128	128	2
6	1/512	128	128	4

N is the number of additional irrotational iterations.

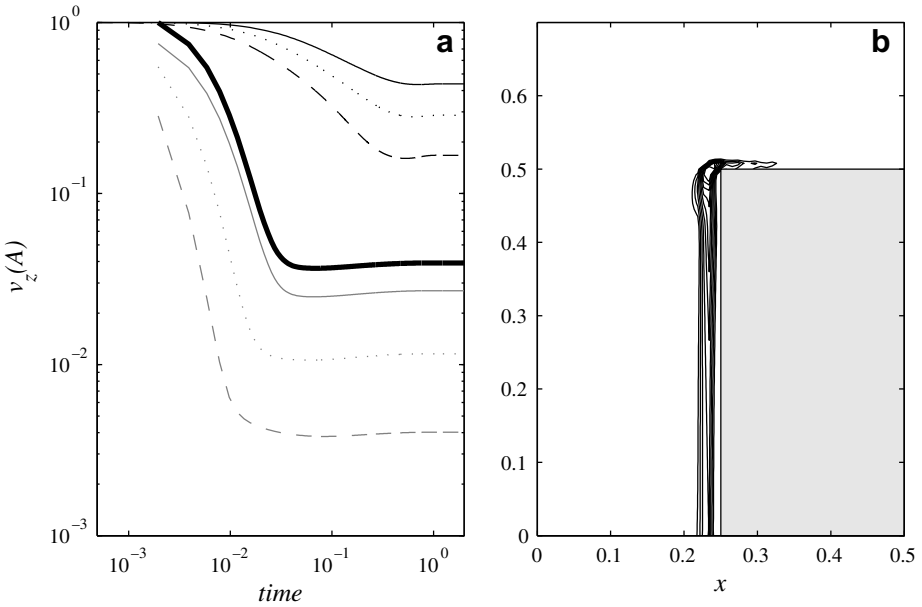

Fig. 7. Test #2. (a) Modulus of v_z at point A. Up to down runs from #1 to #6 in Table 2. Thick line: run #1 of Test #1. (b) Vorticity fields at $t = 4/64$. Contour levels from -200 to -10, step 10.

the upper wall is not negligible, and the lateral flows are consequently reduced for the continuity constraint. The less intense tangential forcing at the lateral walls gives the vorticity field in Fig. 7b, which is substantially different from those in Fig. 2.

3.3. Test #3

The same geometrical problem, with the treatment of the body used in Test #1, has been studied with the unsteady forcing $v_z(x,1) = -\sin(2\pi t/T)$; T has been varied from 1/4 to 2. The velocity at the point A is reported in Fig. 8. When the unsteadiness of the forcing increases, the physical time scale of the problem T approaches the time interval necessary to the numerical convergence of the algorithm detected in the steady Test #1. Increasingly worse solutions are found. The iterative procedure has been applied to the case $T = 1$, improving the solution similarly to what obtained in the steady case.

3.4. Test #4

In this section we analyze the three-dimensional flow inside a prolate spheroid cavity with moving walls [13,14]. The problem is solved using the direct forcing approach in a bi-periodic box. The boundary conditions

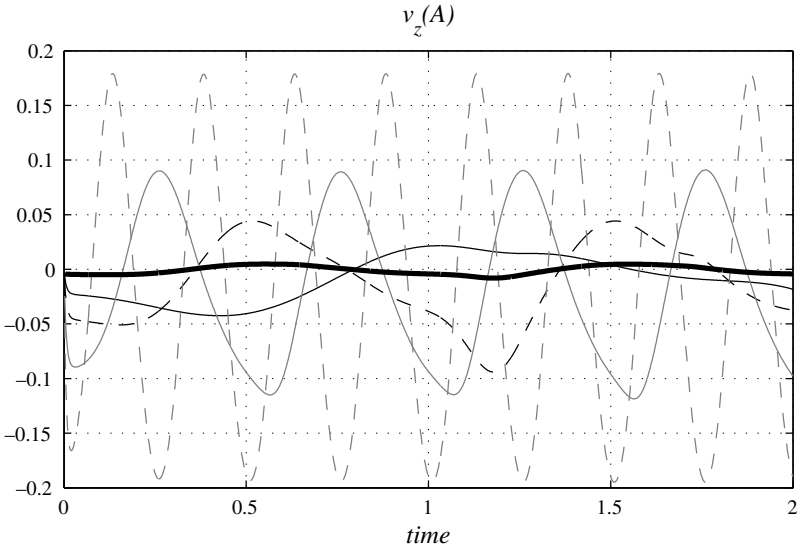

Fig. 8. Test #3. Evolution of the v_z at point A. The numerical parameters are the same of the run #1 of the Test #1. Continuous black, dashed black, continuous gray, dashed gray lines correspond to $T = [2, 1, 1/2, 1/4]$, respectively. The thick line corresponds to the case $T = 1$ with four iterations of the irrotational correction.

are imposed directly at the points closest to the immersed wall, which is therefore described in a stepwise way. Since staggered variables are used, the theoretically thin surface is somehow diffused inside the fluid domain. The mathematical definition of the problem can be found in Domenichini et al. [13]. The Reynolds number in (1) is here replaced by a Stokes parameter $\beta = D^2/\nu T = 225$, being D a reference value of the equatorial diameter and T the period of the forcing motion [14]. The dimensions of the numerical box are $1.5 \times 1.5 \times 1.6$; it has been verified, the results are not reported here, that the solution is substantially not affected by the dimensions of the computational box. Along the periodic directions, N_x and N_y harmonics are used, N_z are the grid points in the z-direction. The same problem has been studied solving the Navier–Stokes equations in the body-fitted system of coordinates with the same standard fractional step method. Details can be found in [13]. In the present case, a grid 64×128 for the meridian plane and 16 harmonics in the azimuthal direction have been used. At the inlet section, $z = 1.6$, the entering velocity profile assigned during the advancement (3) and the conditions imposed solving (4) are the same for the two different codes.

Table 3
Test #4: parameters of the runs. N is the number of additional irrotational corrections

#	N_x	N_y	N_z	N	Δt
1	128	128	128	0	1/512
2	128	128	256	0	1/512
3	256	256	128	0	1/512
4	128	128	128	1	1/512
5	128	128	128	2	1/512
6	128	128	128	4	1/512
7	128	128	128	8	1/512
8	128	128	128	0	1/1024
9	128	128	128	0	1/2048
10[a]	128	128	128	0	1/512
11[a]	128	128	128	2	1/512
12[a]	128	128	128	8	1/512

[a] Runs #10–12 have been performed with a thick wall, as described in the text.

The y-component of the vorticity for some runs in Table 3 at $t = 24/64$ and $y = 0.75$ (vertical mid-plane) are compared in Fig. 9 with the results obtained with the code written in the body-fitted system of coordinates. The jet that enters the expanding cavity has a blunt profile [11], which allows the development of a three-dimensional ring-shaped vortex, whose vertical section is represented by the two counter-rotating vortices in Fig. 9a. The right vortex moves tangentially to the wall, while the left one penetrates transversally occupying the central part of the cavity [13,14]. When the problem is solved with the direct forcing method, the boundary condition at the wall is violated. The different underlying irrotational flow modifies the motion of the vortex structure: the right part does not develop close to the wall, but penetrates more deeply the cavity, the horizontal displacement of the left one is reduced, Fig. 9b. Finer grids, not shown, do not modify the

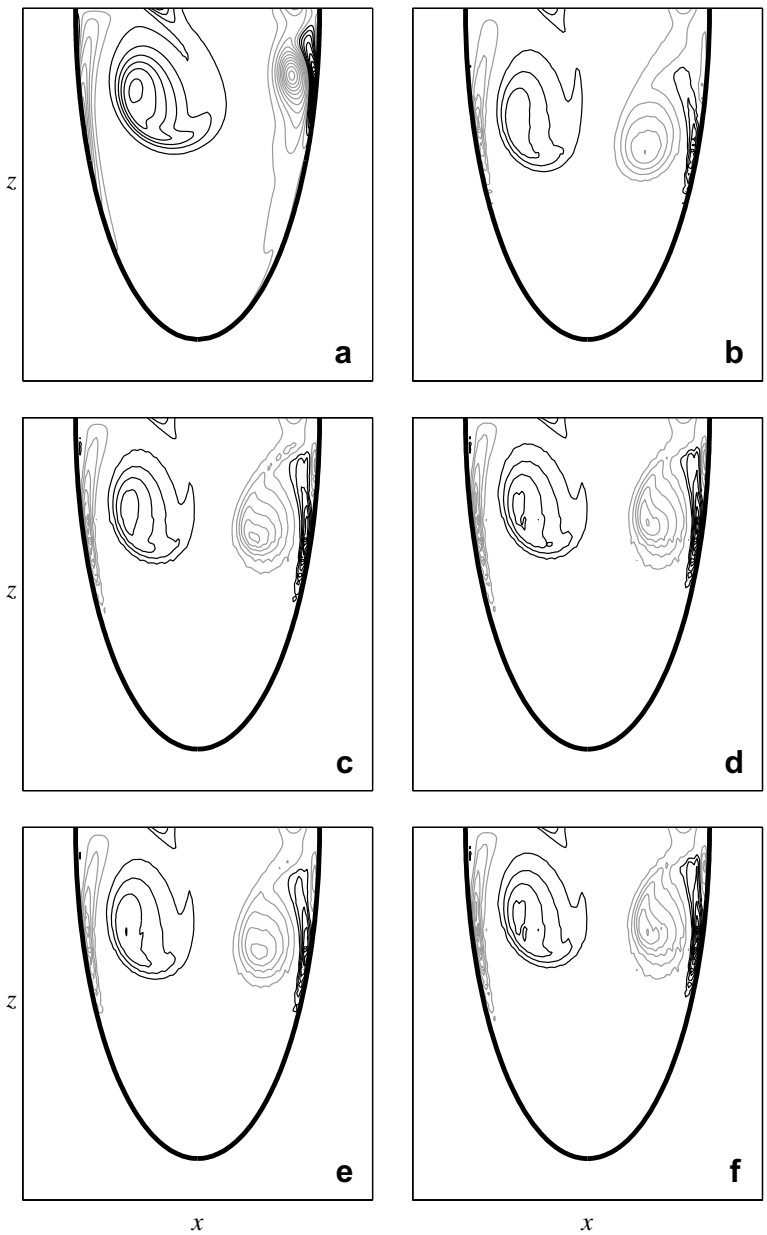

Fig. 9. Test #4. Instantaneous vorticity fields, y-component, at $y = 0.75, t = 24/64$. Contour levels from -105 to 105 and step 10; positive levels: black lines. (a) Body-fitted system of coordinates; (b–f) runs #[1,9,7,10,12] in Table 3, respectively.

results. Previous findings are confirmed: smaller Δt and the iterative procedure drive the flow to the correct solution, Figs. 9c and 9d, respectively. Following the comparison between the results of Test #1 and Test #2, the problem has been solved assuming a thicker wall, Fig. 9e; in this case the wall thickness is four times the step size in the z-direction. This strategy has been coupled with the iterative procedure, Fig. 9f. The field is very similar to that in Fig. 9d, suggesting that the iterations have an impact on the solution more relevant than the treatment of the body.

4. Discussion

In the present work the consistency of the direct forcing approach [9] has been analyzed when a fractional step method is used to solve the Navier–Stokes equation. Simple two-dimensional problems have been defined, avoiding as much as possible interpolating techniques that may affect the discussion.

The central issue of this work is the behavior of the velocity normal to the boundaries when (4) is solved straightforwardly. Such an approach does not have any theoretical support, and numerical arguments do not give satisfactory explanations about its correctness, when it is used in conjunction with a fractional step method [9]. To overcome this problem, different methods have been developed [10,11] that can not be implemented when spectral methods are used, as in the present case.

If any additional condition is imposed during the solution of (4) and the computation of (6), the resulting velocity field violates the impenetrability of the walls, as expected from the mathematical nature of the problem. It has been verified that, also in the reference run of the steady Test #1 performed with the coarsest grid, the relative modification induced by the normal correction, say $(\boldsymbol{v}^* - \boldsymbol{v})/\boldsymbol{v}^* = \mathcal{G}(\phi)/(\boldsymbol{v} + \mathcal{G}(\phi))$, becomes negligible small after few initial steps [9]. However, this is not sufficient to ensure the satisfaction of the boundary condition. The solution reaches an almost steady state, see Figs. 3 and 4: at each time step the momentum equation (3) and the mass conservation (4)–(6) add and subtract alternatively an almost steady error. Improvements was obtained lowering the Δt, in any case well below the values that guarantee the stability of the solution. An alternative procedure is represented by the iterations of the irrotational correction. The meaning of this procedure related to the numerical diffusion of the divergence has been discussed, and an approximate criterion to estimate the number of iterations necessary to lower the errors has been suggested.

Regarding the tangential velocity, it has been shown that the modifications of the velocity field close to rigid walls, due to the violation of their impenetrability, affect the satisfaction of the adherence condition also.

It can be said that the direct forcing approach gives satisfactory results when a qualitative description or the gross features of the solution are required. Additional care in the treatment of the boundaries is necessary when the details of the flow close to walls are a relevant subject of the problem. This appears further important in case of thin boundaries especially when the velocities at both sides of the surface are in the same direction, as detected in the Test #2. An additional source of inconsistency is represented by the unsteadiness of the problem, which can be given by the external forcing, Test #3, by the motion of the boundary, Test #4, or by the internal evolution of the flow.

The proposed method has been applied to two-dimensional problems with sharp-edged solid bodies and to a three-dimensional one with a moving smooth surface. It has been verified that the presence of corners is a very sensitive issue. Thus, further studies are needed to validate the procedure in case of three-dimensional bodies with steep curvature. Moreover, in case of accelerating bodies, when a pressure gradient in the direction normal to the surface is expected to develop naturally, it must be verified the convergence of the method and the absence of numerical instability close to the immersed surfaces.

A final remark must be added about the interpolations, that in the present work have been reduced as much as possible. Several schemes have been suggested employing linear and/or quadratic interpolations of the fluid variables [1]. In case of a fixed two-dimensional wall, if n and τ are the normal and tangential coordinates, respectively, at $n = 0$ the boundary conditions are $u_n = u_\tau = 0$, so that $\partial u_n/\partial\tau = \partial u_\tau/\partial\tau = 0$. Moreover, mass conservation gives $\partial u_n/\partial n = 0$, while in general $\partial u_\tau/\partial n \neq 0$. Thus, at the lower order of approximation we have $u_\tau = C_1 n + C_2 n^2 + O(n^3)$ and $u_n = C_3 n^2 + O(n^3)$ as $n \to 0$. The normal velocity is an infinitesimal of higher order, therefore different interpolations must be used to take into account this point. Analogous considerations hold for the irrotational part of the solution ϕ. In this case, the constraints give $\phi = A + Bn^2/2 + Cn^3/3 + O(n^4)$. Then, if needed, the normal and tangential components of $\nabla\phi$ must be

computed with different interpolations, $u_n = Bn + Cn^2 + O(n^3)$ and $u_\tau = \partial A/\partial\tau|_{n=0} + \partial B/\partial\tau|_{n=0} n^2/2 + O(n^3)$, in order to satisfy the impenetrability condition and the irrotationality of the $\nabla\phi$ field.

Acknowledgement

The author wishes to thank G. Pedrizzetti for many useful discussions. The work has been partially supported by Italian MIUR under the Grant PRIN 2006087719. Finally, the author wishes to thank the referee II for suggesting several improvements of the work, and the referee I for the interesting contribution about the iterative method.

References

[1] R. Mittal, G. Iaccarino, Immersed boundary methods, Annu. Rev. Fluid Mech. 37 (2005) 239–261.
[2] C.S. Peskin, The fluid dynamics of heart valves: experimental, theoretical and computational methods, Annu. Rev. Fluid Mech. 14 (1981) 235–259.
[3] L. Zhu, C.S. Peskin, Simulation of flapping flexible filament in a flowing soap film by the immersed-boundary method, J. Comp. Phys. 179 (2002) 452–468.
[4] R. Verzicco, J. Mohd-Yosuf, P. Orlandi, D. Haworth, LES in complex geometries using boundary body forces, AIAA J. 38 (2000) 427–433.
[5] R. Verzicco, M. Fatica, G. Iaccarino, P. Moin, B. Khalighi, Large-eddy simulation of a road–vehicle with drag reduction devices, AIAA J. 40 (2002) 2447–2455.
[6] E. Balaras, Modeling complex boundaries using external force field on fixed Cartesian grids in large-eddy simulations, Comp. Fluids 33 (2004) 375–404.
[7] M.M. Rai, P. Moin, Direct simulations of turbulent flow using finite-difference schemes, J. Comp. Phys. 96 (1991) 16–53.
[8] R. Verzicco, P. Orlandi, A finite-difference scheme for three-dimensional incompressible flows in cylindrical coordinates, J. Comp. Phys. 123 (1996) 402–414.
[9] E.A. Fadlun, R. Verzicco, P. Orlandi, J. Mohd-Yosuf, Combined immersed-boundary finite-difference methods for three-dimensional complex flow simulations, J. Comp. Phys. 161 (2000) 35–60.
[10] J. Kim, D. Kim, H. Choi, An immersed-boundary finite-volume method for simulations of flow in complex geometry, J. Comp. Phys. 171 (2001) 135–150.
[11] T. Ikeno, T. Kajishima, Finite-difference immersed boundary method consistent with wall conditions for incompressible turbulent flow simulations, J. Comp. Phys. (2007), doi:10.1016/j.jcp.2007.05.028.
[12] G.K. Batchelor, An Introduction to Fluid Dynamics, Cambridge University Press, Cambridge, 1967.
[13] F. Domenichini, G. Pedrizzetti, B. Baccani, Three-dimensional filling flow into a model left ventricle, J. Fluid Mech. 539 (2005) 179–198.
[14] G. Pedrizzetti, F. Domenichini, Nature optimizes the swirling flow in the human left ventricle, Phys. Rev. Lett. 95 (2005) 108101.